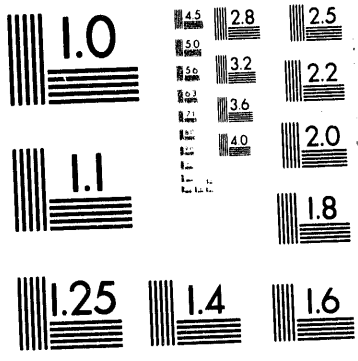
1.0
1.1
1.25
1.4
1.6
1.8
2.0
2.2
2.5
2.8
3.2
3.6
4.0
4.5
5.0
5.6
6.3
7.1
8.0
9.0

1 of 1

DOE/PC/92550--4

EVALUATION OF HYPERBARIC FILTRATION FOR FINE COAL DEWATERING

DOE Grant No. DE-PS22-92PC92520

Fourth Quarterly Technical Progress Report
(June 1, 1993 - September 30, 1993)

by

B.K. Parekh (PI)
University of Kentucky

R. Hogg (Co-PI)
The Pennsylvania State University

A. Fonseca (Co-PI)
Consol Inc.

OBJECTIVES AND SCOPE OF WORK

The main objectives of the project are to investigate the fundamental aspects of particle-liquid interaction in fine coal dewatering, to conduct laboratory and pilot plant studies on the applicability of hyperbaric filter systems and to develop process conditions for dewatering of fine clean coal to less than 20 percent moisture.

The program consist of three phases, namely

Phase I - Model Development

Phase II - Laboratory Studies

Phase III - Field Testing

The Pennsylvania State University is leading efforts in Phase I, the University of Kentucky in Phase II, and Consol Inc. in Phase III of the program. All three organizations are involved in all the three phases of the program. The Pennsylvania State University is developing a theoretical model for hyperbaric filtration systems, whereas the University of Kentucky is conducting experimental studies to investigate fundamental aspects of particle-liquid interaction and application of high pressure filter in fine coal dewatering. The optimum filtration conditions identified in phase I and II will be tested in a Consol Inc. coal preparation plant using an Andritz Ruthner portable hyperbaric filtration unit.

INTRODUCTION

Most of the coal presently used by the utility industry is cleaned at preparation plants employing wet processes. Water, while being the mainstay of coal washing, is also one of the least desirable components in the final product. Coarse coal (+3/4 inch) is easily dewatered to a 3-4 percent moisture level using conventional vibrating screens and centrifuges. However, the main problem of excess product moisture occurs in fine (minus 28 mesh) coal and refuse. Even though fines may constitute only about 20 percent of a contemporary cleaning plant feed, they account for two-thirds of the product surface moisture. This high surface moisture offsets many of the benefits of coal cleaning, and can easily undercut the ongoing programs on recovery of fine clean from refuse as well as producing an ultra-fine super clean coal fuel.

Currently, most of the coal preparation plants utilize vacuum disk or drum filter technology for dewatering of the fine coal, providing dewatered product containing about 25 percent moisture. The coal industry would prefer to have a product moisture in the range of 10 to 15 percent. Although the desired product quality can be obtained using thermal dryer, there are problems associated with this technology such as high capital costs and the greatest potential source of air pollution in a coal cleaning plant.

In the present research project, an alternative to thermal drying, hyperbaric filtration which has shown potential in lowering moisture content in fine coal to less than 20 percent level, is being investigated in detail. The project will develop fundamental information on particle-liquid interaction during hyperbaric filtration and apply the knowledge in developing optimum conditions for the pilot plant testing of the

hyperbaric filter system.

APPROACHES AND PROGRESS

PHASE I Model Development

Dewatering Model

The framework of a model for filter cake dewatering by gas displacement was described in previous reports (March, 1993, June 1993) and can be summarized as follows:

1. Starting from an initially fully-saturated cake, liquid is driven out of individual pores in response to the applied gas pressure. Since the principal resistance to flow is provided by the liquid in the pores, the effective pressure gradient is assumed to be

$$\frac{\Delta P}{(L-z)} = \frac{\Delta P_o - P_c}{(L-z)} \qquad (1)$$

where ΔP_o is the applied pressure differential across the cake, P_c is the capillary pressure in the pores, L is the cake thickness and z is the distance from the liquid-gas interface to the upper (high pressure) surface of the cake. Because the length (L-z) of the remaining liquid in the pore decreases as the pore empties, the flow velocity actually increases as dewatering proceeds.

2. At some time t_B, the liquid in the largest pores (radius r_m) is completely expelled and gas breaks through the cake. It was shown in the previous report that the breakthrough time can be estimated from

$$t_B = \frac{4\mu L^2}{\Delta P_o r_m (r_m - r^*)} \quad (2)$$

where μ is the liquid viscosity and r* is defined by

$$r^* = \frac{2\gamma \cos\theta}{\Delta P_o} \quad (3)$$

and represents the pore radius for which the applied and capillary pressures are equal.

In practice, breakthrough times are generally very short (<<1 sec) and breakthrough occurs before significant dewatering has been achieved.

For pores smaller than r_m, the remaining saturation S_B can be obtained based on the flow analysis outlined in the previous (June 1993) report. Thus for a pore of radius r ($<r_m$),

$$S_B = 1 - \frac{z_B}{L} \quad (4)$$

where Z_B is the location of the interface at breakthrough in the largest pore (time t_B). From the flow analysis (Equation 4 of June 1993 report).

$$z_B(2L - z_B) = \frac{r^2(\Delta P_o - P_c)}{4\mu} t_B \quad (5)$$

Combination of Equations 2, 3, 4 and 5 leads to

$$S_B = \sqrt{\frac{r_m - r}{r_m - r^*}} \qquad (6)$$

3. Once gas breakthrough has occurred in the largest pores, flow through such pores leads to a linear pressure gradient along the pore. Assuming that all pores in the bed are completely interconnected, the pressure in any pore at location z must be the same so that the linear pressure gradient exists over the entire bed. This is in contrast to the situation prior to initial breakthrough, where it is considered that there is essentially no pressure drop in the empty portion of the pore (0 to z) and the entire gradient occurs over the filled portion (z to L), as described by Equation 1.

From the above reasoning, the pressure gradient in the liquid in a partially filled pore, after initial breakthrough is given by

$$\frac{\Delta P}{(L-z)} = \frac{\Delta P_o}{L} - \frac{P_c}{L-z} \qquad (7)$$

As dewatering proceeds and z approaches L, the second term in Equation 7 increases until the effective gradient becomes zero. At this point, i.e. when

$$\frac{\Delta P_o}{L} = \frac{P_c}{L-z} \qquad (8)$$

flow through the pore ceases. The relative filling of the pore (residual saturation S_∞) is (L-z)/L. Then, from Equation 8,

$$S_\infty = \frac{P_c}{\Delta P_o} \tag{9}$$

and, from the definition:

$$P_c = \frac{2\gamma\cos\theta}{r} \tag{10}$$

$$S_\infty = \frac{2\gamma\cos\theta}{r\Delta P_o} \tag{11}$$

or, using Equation 3,

$$S_\infty = \frac{r^*}{r} \tag{12}$$

Equation 12 defines the limits of dewatering for pores of radius r at applied pressure ΔP_o.

Kinetics of Dewatering

In the previous (June 1993) report it was shown that the flow velocity through a pore can be expressed by

$$v = \frac{dz}{dt} = \frac{r^2\Delta P}{8\mu(L-z)} \tag{13}$$

Following initial breakthrough, the pressure gradient is given by Equation 7 so that Equation 13 becomes

$$\frac{dz}{dt} = \frac{r^2 \Delta P_o}{8\mu L} - \frac{\gamma r \cos\theta}{4\mu(L-z)} \quad (14)$$

Defining, as before, the saturation S as

$$S = 1 - \frac{z}{L} \quad (15)$$

Equation 14 can be written

$$\frac{dS}{dt} = \frac{\gamma r \cos\theta}{4\mu L^2 S} - \frac{r^2 \Delta P_o}{8\mu L^2} \quad (16)$$

Defining a dimensionless time variable T such that

$$T = \frac{r^2 \Delta P_o t}{8\mu L^2} \quad (17)$$

and making use of Equations 3 and 7, Equation 16 can be reduced to

$$\frac{dS}{dT} = \frac{S_\infty}{S} - 1 \quad (18)$$

The appropriate initial condition is that at $t=t_B$, $T=T_B$, and $S=S_B$, where t_B is the initial breakthrough time given by Equation 2, T_B is the corresponding value of T and S_B is given by Equation 6. Integration of Equation 18 then leads to

$$S_B - S - S_\infty \ln\left(\frac{S-S_\infty}{S_B-S_\infty}\right) = T - T_B \quad (19)$$

Equation 19 describes the kinetics of liquid removal from pores of radius r. Some examples, are given in Figures 1 and 2. The role of pore size is illustrated in

Figure 1 which clearly demonstrates the importance of this variable with regard to both the rate of dewatering and the limiting saturation that can be achieved. For these particular conditions, the critical pore radius, r^*, is about 0.6 μ m; smaller pores cannot be dewatered at this pressure (30 psi). Figure 2 shows the effect of applied pressure on the removal of water from 1 μ m pores. The advantages of hyperbaric filtration over conventional vacuum filtration (ΔP_o<14 psi) are readily apparent. Again, it can be seen that increased pressure provides both increased dewatering rates and reduced limiting saturation. Dewatering is only possible, for these 1 μ m pores if the applied pressure is greater than about 18 psi; vacuum filtration would be completely ineffective.

Equation 19 describes the process of dewatering for systems of uniform pores. For real systems, it is necessary to integrate over the range of pore sizes present. Thus, the overall saturation S_T at any time must be obtained using

$$S_T = \int_0^{r_m} S(r)f(r)dr \qquad (20)$$

where f(r) represents the pore size distribution, defined such that

f(r)dr = volume fraction of pores whose radius lies between r and r + dr.

The quantity S(r) must be obtained from solutions to Equation 19. Because of the form of this equation, which cannot be inverted to give an explicit relationship for S(t), numerical procedures involving root-finding techniques must be employed. This aspect of the work is currently in progress.

Overall Limiting Saturation

In the June 1993 report, it was shown that, for the case of the limiting saturation, Equation 20 reduces to

$$S_{TL} = r \cdot \int_{o}^{r_m} \frac{f(r)dr}{r} \qquad (21)$$

While the form of the pore size distribution is not usually known, the integral in Equation 21 can be evaluated from a knowledge of the particle size distribution. If the total pore volume is V_p, the volume of pores which have radius r to r+dr is $V_p f(r)dr$. The total length of such pores is

$$d\ell = \frac{V_p f(r)dr}{\pi r^2} \qquad (22)$$

The surface area of a pore of radius r and length $d\ell$ is

$$dA = 2\pi r d\ell \qquad (23)$$

so that, from Equation 22

$$dA = \frac{2V_p f(r)dr}{r} \qquad (24)$$

and the total pore surface area is

$$A = 2V_p \int_{o}^{r_m} \frac{f(r)dr}{r} \qquad (25)$$

The bed porosity ε is defined by

$$\varepsilon = \frac{V_p}{V_p + V_s} \tag{26}$$

where V_s is the total volume of solid. Equation 26 can be solved for V_p giving

$$V_p = (\frac{\varepsilon}{1-\varepsilon})V_s \tag{27}$$

Substitution into Equation 25 leads to

$$\frac{A}{V_S} = \frac{2\varepsilon}{(1-\varepsilon)}\int_o^{r_m} \frac{f(r)dr}{r} \tag{28}$$

If particles in the cake are in contact at points only, the pore surface area is equal to the particle surface area and the quantity A/V_s represents the volume specific surface area S_v of the solids in the cake. Specific surface areas can be obtained from simple measurements such as the well-known Blaine test.

Combination of Equations 21 and 28 leads to the following simple expression for the limiting filter-cake saturation:

$$S_{TL} = \frac{S_v(1-\varepsilon)\gamma\cos\theta}{\varepsilon\Delta P_o} \tag{29}$$

The corresponding limiting moisture content can be estimated using

$$M_L = \frac{\rho_\ell S_v \gamma\cos\theta}{\rho_\ell S_v \gamma\cos\theta + \rho_s \Delta P_o} \tag{30}$$

where ρ_ℓ and ρ_s are the liquid and solid densities, respectively. It should be emphasized that the moisture content M_L as given by Equation 30 is the limiting value which is approached after long dewatering times. Filter cakes which include a large

fraction of pores close to the critical size r^* may require very long times for this level to be attained.

PHASE II Laboratory Studies

The coal used during this period was froth flotation product sample of Illinois No.6 supplied by Consolidation Coal Inc. The main accomplishments during this period included investigations of the effects of addition of flocculants, surfactants and combinations of metal ions and surfactants on final moisture content of the filter cakes. The investigation included assessment of the effects of type of additive (anionic, nonionic and cationic), establishment of optimum dosage of additives and examination of surface chemical properties of the coal with and without presence of additives. All of the experiments reported were carried out using the optimum filtration conditions, i.e. applied pressure of 60 psi with a cake thickness of 2.0 cm and a filtration time of 2 minutes.

Effect of Flocculants on Dewatering

The experiments on effects of flocculant addition on dewatering behavior were conducted using flocculant dosage of 5 to 50 ppm to determine the optimum concentration of flocculants. Three types of flocculants with the same molecular weight and ionic charge density obtained from American Cyanamid Co. were used in flocculant-assisted filtration studies. Data on these flocculants are listed in Table 1 according to type, molecular weight and relative charge density. All these flocculants were dissolved in distilled water to prepare stock solutions of 0.1 weight percent

concentration.

The effectiveness of a flocculant depends on the mixing conditions of slurry and flocculant. The effect of mixing conditions was studied using 20 ppm of Superfloc 204 Plus at different flocculation times and various agitation speeds. The effect of agitation speed was studied in the range of 300 to 1500 rpm for 110 seconds flocculation time. Figure 3 shows the effect of agitation speed on cake moisture and cake permeability, which indicates that 1000 rpm agitation speed was sufficient to provide lowest filter cake moisture and highest cake permeability. Agitation speed higher than 1000 rpm increased moisture in the filter cake, which may be due to breakage of flocs. In another set of experiments the agitation speed was kept constant at 1000 rpm and flocculation time varied from 5 to 240 seconds. The final moisture content and permeability of cake as a function of flocculation time are shown in Figure 4. An optimum flocculation time was observed at about 110 seconds which

Table 1. List of Flocculants Investigated

Name	Type	Molecular Weight million	Charge Density mol. %
Superfloc 204 Plus	Anionic	4 - 6	35
Superfloc 16	Nonionic	4	0
Magnifloc 494C	Cationic	4	35

lead to both higher cake permeability and lower cake moisture. All the tests data reported here-in on flocculant-assisted filtration were conducted using agitation speed of 1000 rpm and flocculation time of 110 seconds.

To determine the optimum dosage and the influence of the type of flocculant experiments were conducted using flocculant concentration in the range of 5 to 50 ppm. The experimental results are illustrated in Figure 5, which shows that for the anionic flocculant, the optimum dosage was about 30 ppm at which the final moisture content of the filter cake was 17 percent, which was about five percent lower than that of the untreated filter cake. For the nonionic and cationic flocculants, the optimum dosages were found to be 20 and 10 ppm, respectively. At these dosages, the final cake moisture obtained for both the flocculants was about 19 percent.

The anionic flocculant was found to perform satisfactorily over the range of flocculant dosage investigated. The reason for the effectiveness of the anionic flocculant is probably the presence of relatively high amounts of calcium and magnesium ions in recycled washery waters which provides linkages for anchoring polymer anionic functional groups to the coal surface. This leads to tight bonding for the flocculation of particles resulting in a fast filtration rate and small residual moisture contents of the filter cake.

Effect of Surfactants on Dewatering

A number of dewatering tests were conducted using anionic (sodium 2 -ethylhexyl sulfate), nonionic (octyl phenoxy polyethoxy ethanol) and cationic (cetyl pyridium chloride) surfactants. Table 2 lists basic information on the three surfactants.

Table 2. List of Surfactants Investigated

Surfactant	Sodium 2-Ethylhexyl Sulfate	Octyl Phenoxy Polyethoxy Ethanol	1-Hexadecyl Pyridinium Chloride
Type	Anionic	Nonionic	Cationic
Commercial Name	NAS 08	Triton X-114	Cetyl Pyridium Chloride
Active Ingredient weight, %	40	100	100
Formula	$C_4H_9(C_2H_5)CH_2$-SO_4Na	C_8H_{17}-C_6H_4-$(OCH_2CH_2)_{7-8}OH$	$C_{16}H_{33}C_5H_5NCl$
Molecular Weight	232	536	340
Manufacturer	Niacet Corporation Niagara Fall, NY	Rohm and Hass Philadelphia, PA	Sigma Chemical St. Louis, MO

Several experiments were performed using surfactant concentration ranging from 5 to 800 mg/liter of slurry to determine the influence of surfactant dosage and the type of surfactant on filtration properties of coal fines. The results for surfactant dosage versus cake moisture are shown in Figure 6. The data show that all surfactants yield cake moisture levels lower than the 21.8 weight percent, which was the observed cake moisture without surfactant. These results indicated that for all surfactants there exist an optimum dosage resulting in a minimum residual filter cake moisture. The optimum dosages were found to be 250, 126 and 380 mg/liter of slurry for the anionic, nonionic and cationic surfactants, respectively. At these dosages, the final moisture contents of the filter cake were 20.0, 18.2 and 16.9 percent for the

anionic, nonionic and cationic surfactants, respectively. The cationic surfactant was found to perform better than the other two surfactants over the wide range of surfactant concentrations investigated.

The widely accepted mechanism of enhanced dewatering by surfactants is reduction of surface tension of suspension, and adsorption of surfactants from solution onto the coal particles. In order to test which one of these phenomena might be controlling the dewatering process, the surface tension of the original surfactant solution and filtrate were measured. Surface tension was measured by the du Nouy ring method, using Fisher Surface Tensiomat Model 21. The results for surfactant dosage versus surface tension of the surfactant solution and filtrate are also shown in Figure 6. Surface tension of the anionic solution did not change even after it was brought in contact with coal, showing no adsorption on coal surfaces as indicated by Figure 6(a). In contrast, surface tension of the filtrate from the nonionic and cationic surfactants was substantially higher than the surfactant solution, itself as shown in Figures 6(b) and 6(c), respectively. This is a clear indication that the nonionic and cationic surfactants are adsorbing on the coal surface. Figures 6(b) and 6(c) for the nonionic and cationic surfactants show that the surface tension of filtrate decreases continuously, the moisture content of the dewatered cake decreases to a certain point of surfactant concentration. Beyond this concentration the cake moisture begins to increase. Therefore, the effect of the addition of surfactants on the residual filter cake moisture cannot be related directly to the lowering of the liquid-air interfacial tensions. This implies that besides decrease in surface tension, the adsorption of surfactants on

coal also plays an important role in changing the dewatering characteristics of filter cakes.

Effect of Metal Ions on Dewatering

Dewatering Studies were conducted using di and tri-valent metal ions to utilize the basic surface-colloid chemistry principle of lowering the zetal potential of coal particles through adsorption of surfactants and metal ions for effective removal of moisture from fine clean coal. The metal ions used in this study are copper and aluminum. Usually, for a given solid-metal ion suspension three charge reversal points (Point of Zero Charge) are observed as pH is varied from acid to alkali side, as shown in Figure 7. CR1 corresponds to the point of zero charge (PZC) of the substrate surface, CR2 corresponds to the pH where formation of the hydroxy species takes place onto the substrate while CR3 is the PZC of the metal hydroxide itself.

Electrophoretic mobility measurements were made on the coal with and without presence of metal ions using the Zeta Meter Model 3.0. The results for electrophoretic mobility of coal without presence of metal ion and final cake moisture are shown as a function of pH in Figure 8. Point of zero charge (PZC) of the coal was found to be pH 3.0. Below the PZC, the particles were positively charged while above the PZC, the particles were negatively charged. Note, that filter cake moisture lowers in the region of PZC as shown in Figure 8(b). However, the improvement in moisture content of the filter cake was not significant.

The electrophoretic mobility of coal in the presence of copper ions with three different concentrations is presented in Figure 9(a). In the presence of 10^{-4} M and

10^{-5} M copper ions CR1 was found to be about pH 3.0 which is the same PZC as for the coal alone. The concentration of 10^{-4} M exhibits an PZC near pH 6 which corresponds to CR2 for copper or the precipitation pH of $Cu(OH)_2$. Above pH 6.0 the coal reveals a maximum positive charge at pH 7.5 and become less positively charged as the pH increases to 11, the PZC of $Cu(OH)_2$ or CR3. Figure 9(a) also shows that copper ion concentration plays a significant role in charge reversal phenomena since the amount of metal hydroxy produced and adsorbed is a function of the amount of metal ions present in solution. Accordingly, the copper ion concentration affects the PZC of $Cu(OH)_2$ or CR3, i.e., lowering concentration leads the CR3 to a slightly lower pH. Results of filtration in the presence of copper ions with three different dosages is shown in Figure 9(b). Most noteworthy is that lower cake moisture obtained near pH between 3.5 and 6.0, and at pH 10.0 which correspond to CR2 and CR3, respectively for copper ions.

In the presence of Al^{+3} ions similar phenomena were observed. As shown in Figure 10(a), CR1 was observed to be pH 3.0 in the presence of 10^{-5} M Al ions, which was the same PZC of coal alone. The coal particles were positively charged below pH 7.5 at the concentrations of 10^{-3} M and 10^{-4} M aluminum ions due to the adsorption of aluminum hydroxy species such as $Al(OH)^{+2}$ and $Al(OH)_2^{+}$. A minima occurred for these concentrations near pH 4.5 which corresponds to CR2, the precipitation pH of $Al(OH)_3$. Even though there was a minimum value of electrophoretic mobility for coal, charge reversal did not take place at these concentrations. The coal particles exhibit a PZC near pH 8.0 which is CR3 or the PZC of $Al(OH)_3$ and were negatively

charged from pH 8.0 to pH 11.5. As in the case with copper ions, the aluminum ion concentration plays a important role in charge reversal phases by determining the amount of $Al(OH)_3$ available for adsorption. Figure 10(b) presents the results of filtration in the presence of various concentrations of aluminum ions. The lowest cake moistures were achieved near pH 4.5 and pH 8.0 which corresponds to CR2 and CR3, respectively for aluminum ions. Like the copper ions, the cake moistures obtained were no more than 2 percent lower than that observed in the absence of metal ions.

Combined Effect of Metal Ions and Surfactants

The mechanism of both surfactants and metal ions addition to the filtration slurry is to increase the hydrophobicity of the substrate by surfactant adsorption while conducting filtration at the PZC of the substrate where electrostatic repulsive forces are minimized and thus micro-flocs of fine coal particles are formed. For electrokinetic property measurements of coal, surfactants and metal ions were prepared in a solution of NaCl to maintain constant ionic strength. A small quantity of colloidal coal particle slurry was added to these solutions. The eletrophoretic mobility was measured using the Zeta Meter at adjusted pH.

The results for electrokinetic properties of coal obtained with copper ions and each of three different types of surfactants are presented in Figure 11. With anionic and nonionic surfactants alone, the electrophoretic mobility was found to be similar to that of coal alone. When both anionic and nonionic surfactants and copper ions were present, the electrophoretic mobility was essentially the same as for copper ions alone as shown in Figures 11(a) and 11(b). This is due to the fact that below pH 5, Cu^{+2} is

present as a predominant ionic species, and other ionic and polymeric species exit in lower concentrations whlie above pH 5, $Cu(OH)_2$ appears to dominate the system and determine the electrokinetic behavior of the coal particles. On the other hand, cationic surfactant and copper ions exhibited quite different electrokinetic behavior as shown in Figure 11(c). Unlike the anionic and nonionic surfactant systems, the electrophoretic mobility of the combined copper ions and cationic surfactant was not affected by the presence of copper hydroxy species. The electrokinetic behavior of the copper ion and cationic surfactant system was observed to be quite close to that of the cationic surfactant alone. These data suggest that the surfactant adsorption dominates the coal surface properties and the effects of $Cu(OH)_2$ are minimized or neutralized.

When aluminum ions and anionic and nonionic surfactants were present, the system showed virtually the same electrokinetic behavior as for aluminum ions alone with the exception of shift of CR3 from pH 8.0 to pH 9.0 as shown in Figures 12(a) and 12(b). The cause of this shift in CR3 can be attributed to the formation of a complex species of $Al(OH)_3$ and the surfactants which exhibits a different PZC. The measurement of electrophoretic mobility of $Al(OH)_3$ precipitated in the presence of the surfactants showed that the PZC of the complex species occurred near pH 9.5. The electrophoretic mobility of coal in the presence of aluminum ions with cationic surfactant is shown in Figure 12(c). As was the case for copper ions, cationic surfactant and aluminum ions interact to minimize or prevent the adsorption of $Al(OH)_3$ by adsorption of cationic surfactant which is significant enough to diminish the effects

of $Al(OH)_3$.

To determine the optimum amount of surfactant needed in combination with metal ions to provide a low moisture filter cake, experiments were performed on varying amounts of surfactants while keeping metal ions (Cu^{+2} and Al^{+3}) concentration constant at 0.25 kg/ton. Figure 13 shows the effect of three different types of surfactants with various metal ions on cake moisture contents. The slurry pH for filtration used in these experiments were 10 and 8 for copper and aluminum ions, respectively which correspond to the PZC of metal hydroxide. With aluminum ions, lowest cake moisture of 19.7 weight percent was obtained with anionic surfactant at dosage of 1.0 kg/ton. However, there was no noticeable advantage in filter cake moisture reduction with metal ions over the entire range of either nonionic and cationic surfactant concentrations. It is evident from these results that addition of the surfactant alone, which either reduces surface tension or makes the coal surface more hydrophobic, was more effective to remove the cake moisture than that of metal ions alone, in particular, for Illinois No.6 coal which contains large particles (about 45 weight percent of +100 mesh particles). This may be due to the fact that dosage of metal ions is not enough to make large flocs among the larger size coal particles.

PHASE III Field Testing

No activities were conducted.

FUTURE WORK

- Baseline dewatering study with the Pittsburgh seam coal froth will be conducted using vacuum as well as high pressure bench scale equipments. The variables to be studied will be driving force, filtration time, cake thickness, slurry concentration and pH.
- Statistical experimental design on baseline dewatering study will be employed to identify significant variables and to optimize process condition.

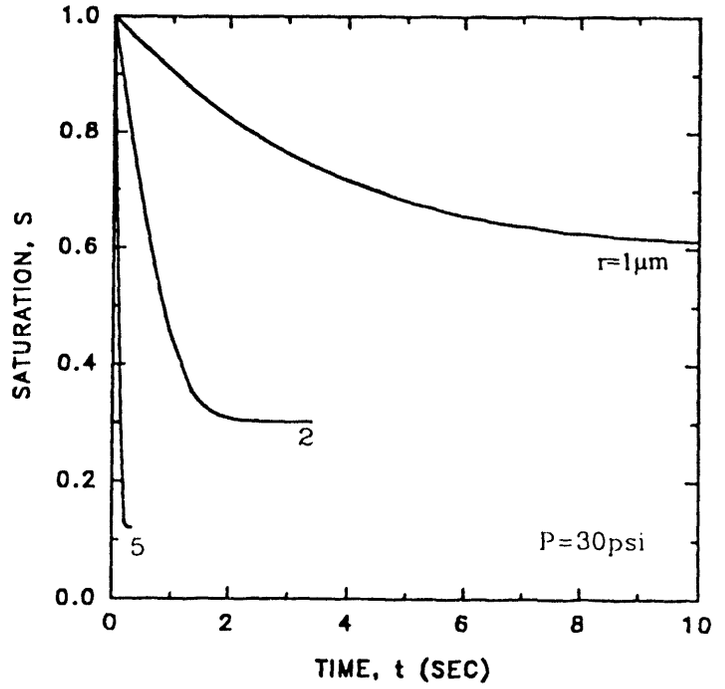

Figure 1. Kinetics of dewatering in pores of varying radius at an applied pressure of 30 psi (γ =72 dynes/cm, θ =30 degree)

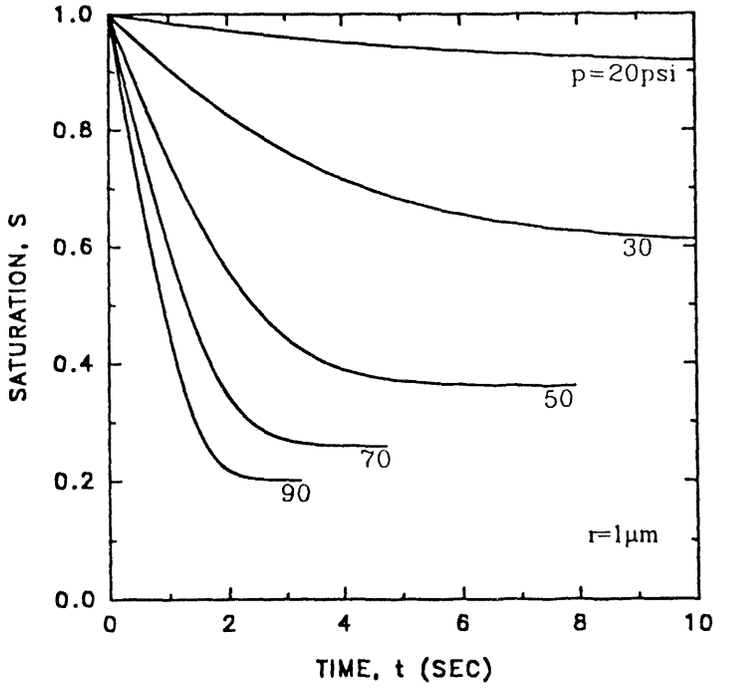

Figure 2. Effect of applied pressure on dewatering kinetics in 1 μ m radius pores (γ =72 dynes/cm, θ =30 degree)

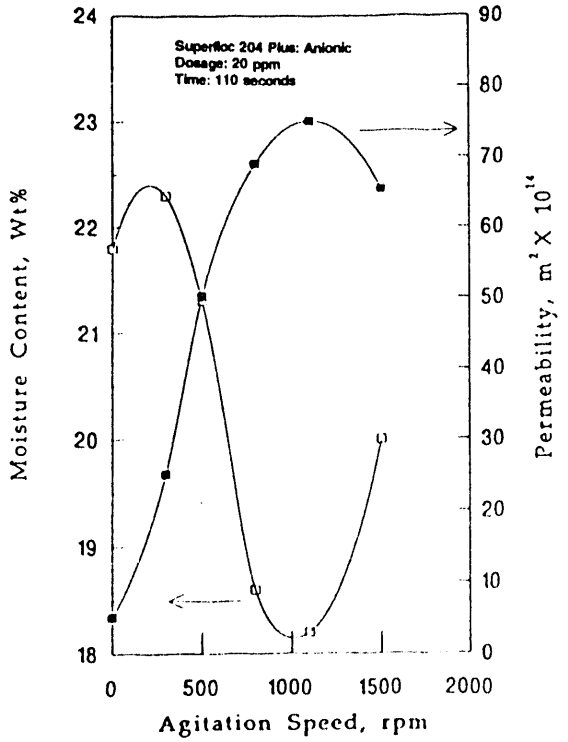

Figure 3. Effect of agitation speed on cake moisture and permeability

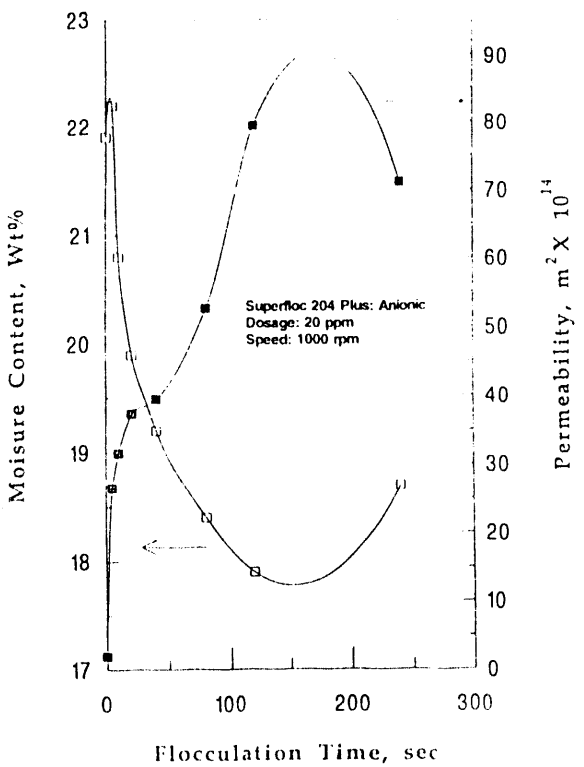

Figure 4. Effect of flocculation time on cake moisture and permeability

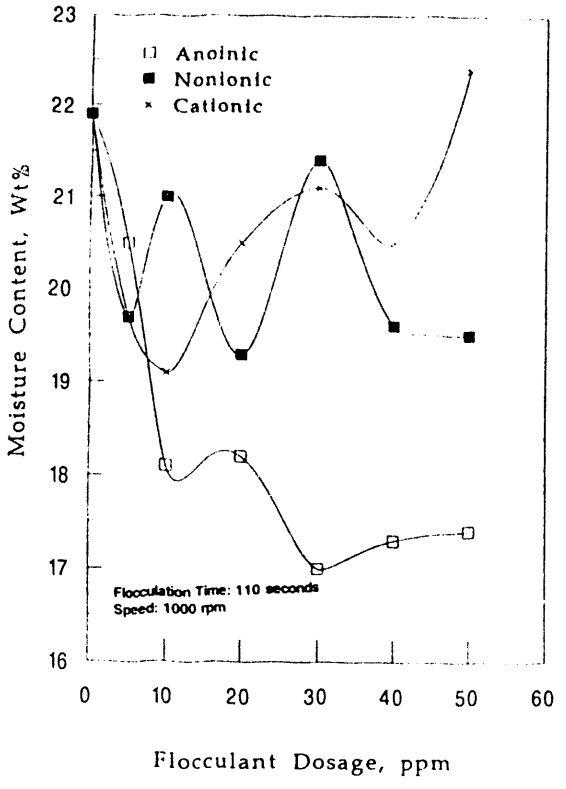

Figure 5. Effect of flocculant dosage on cake moisture

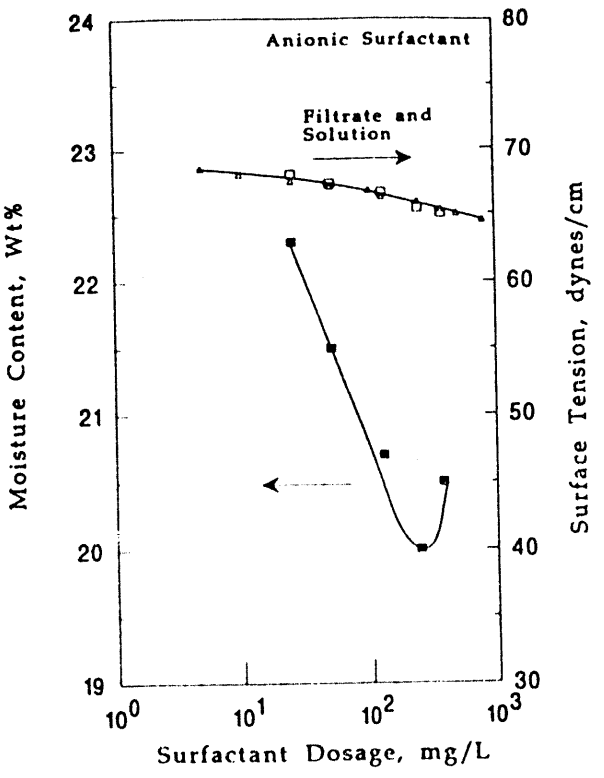

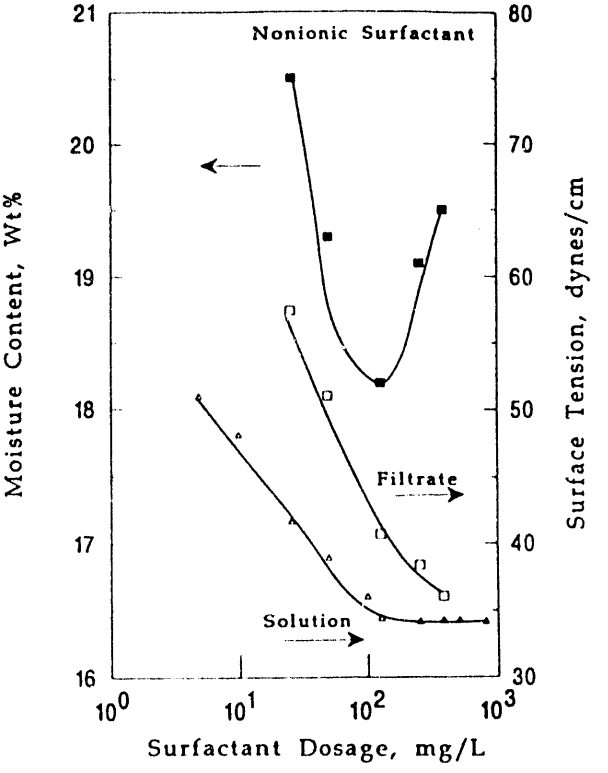

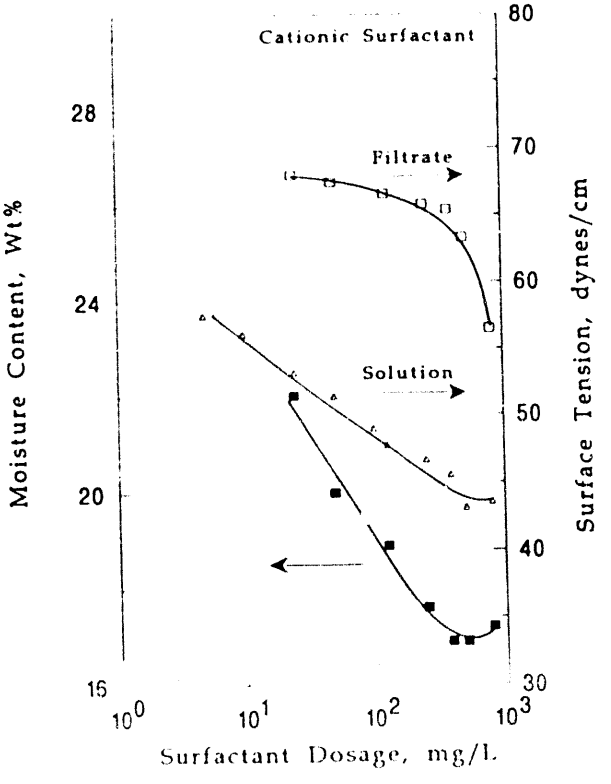

Figure 6. Effect of surfactant dosage on cake moisture and surface tension of filtrate and solution

(a) Anionic surfactant

(b) Nonionic surfactant

(c) Cationic surfactant

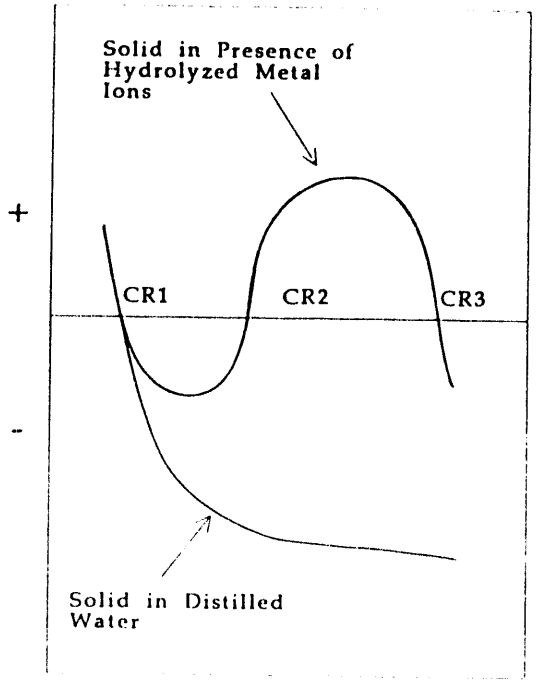

Figure 7. Charge reversal of solid with and without presence of metal ions

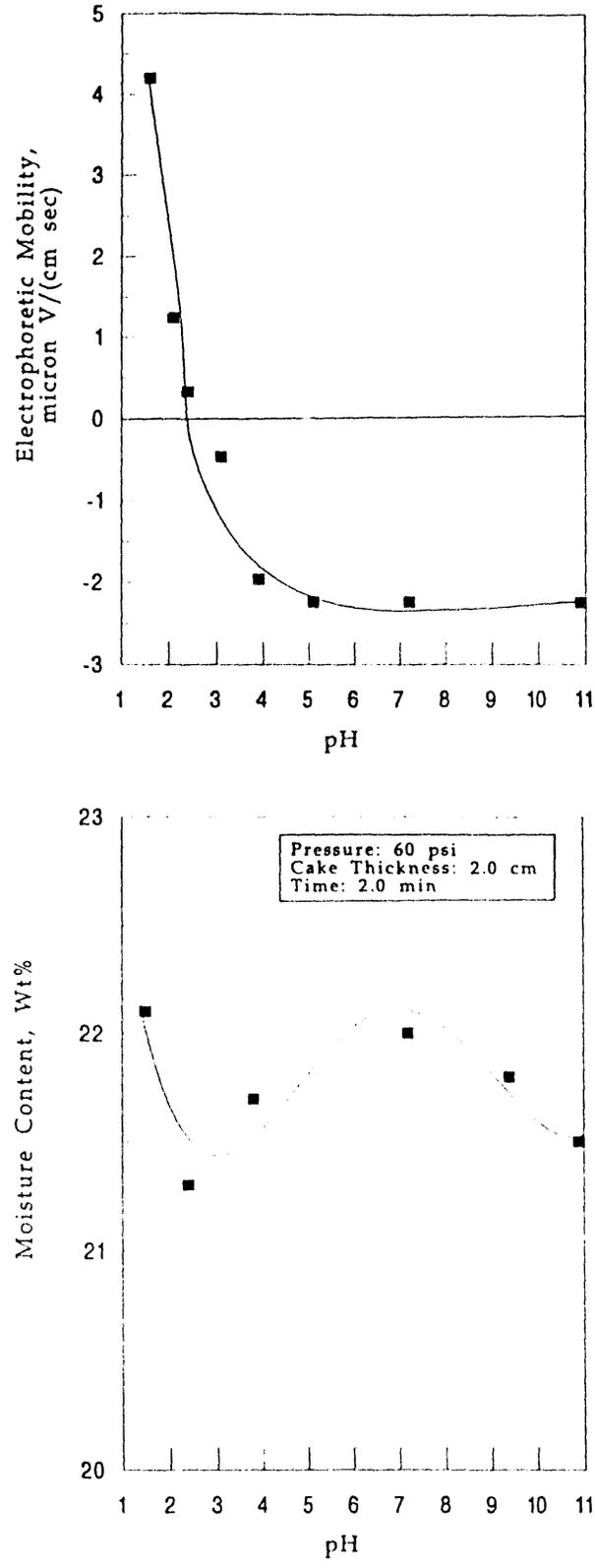

Figure 8. Effect of pH without presence of metal ions

(a) Electrophoretic mobility

(b) Cake moisture

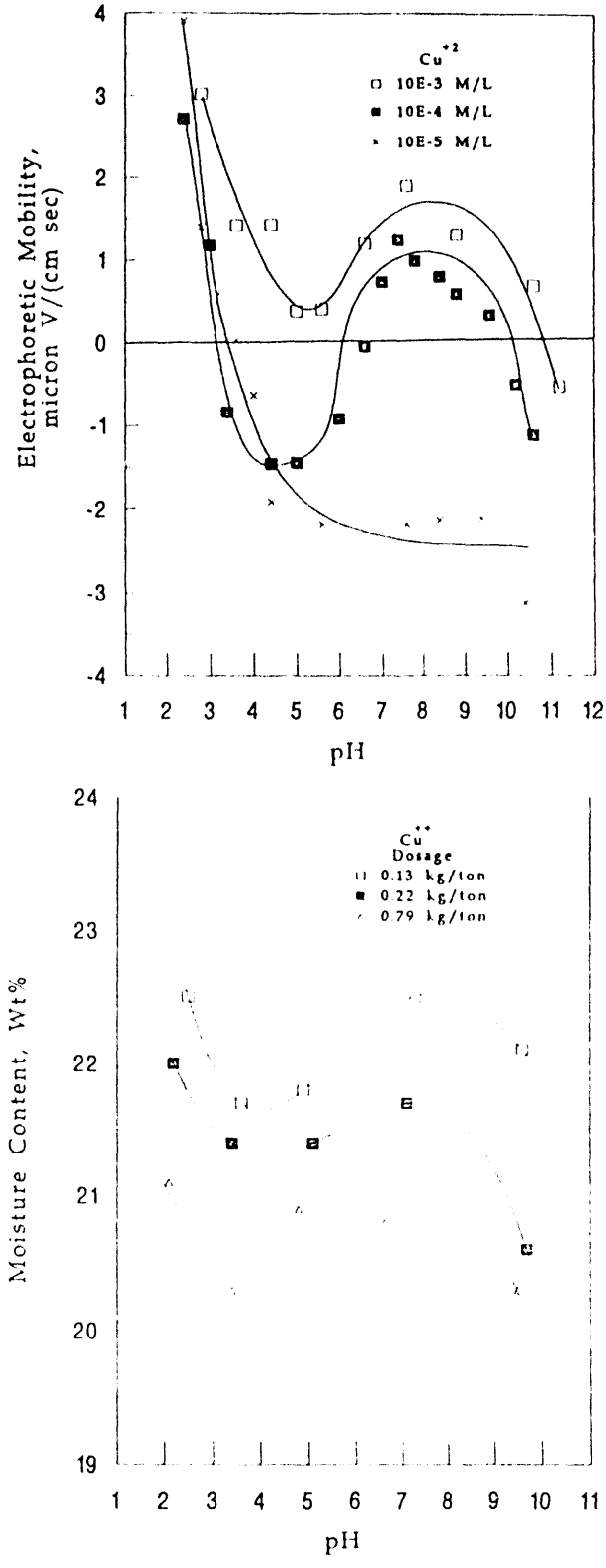

Figure 9. Effect of pH with presence of copper ions

(a) Electrophoretic mobility

(b) Cake moisture

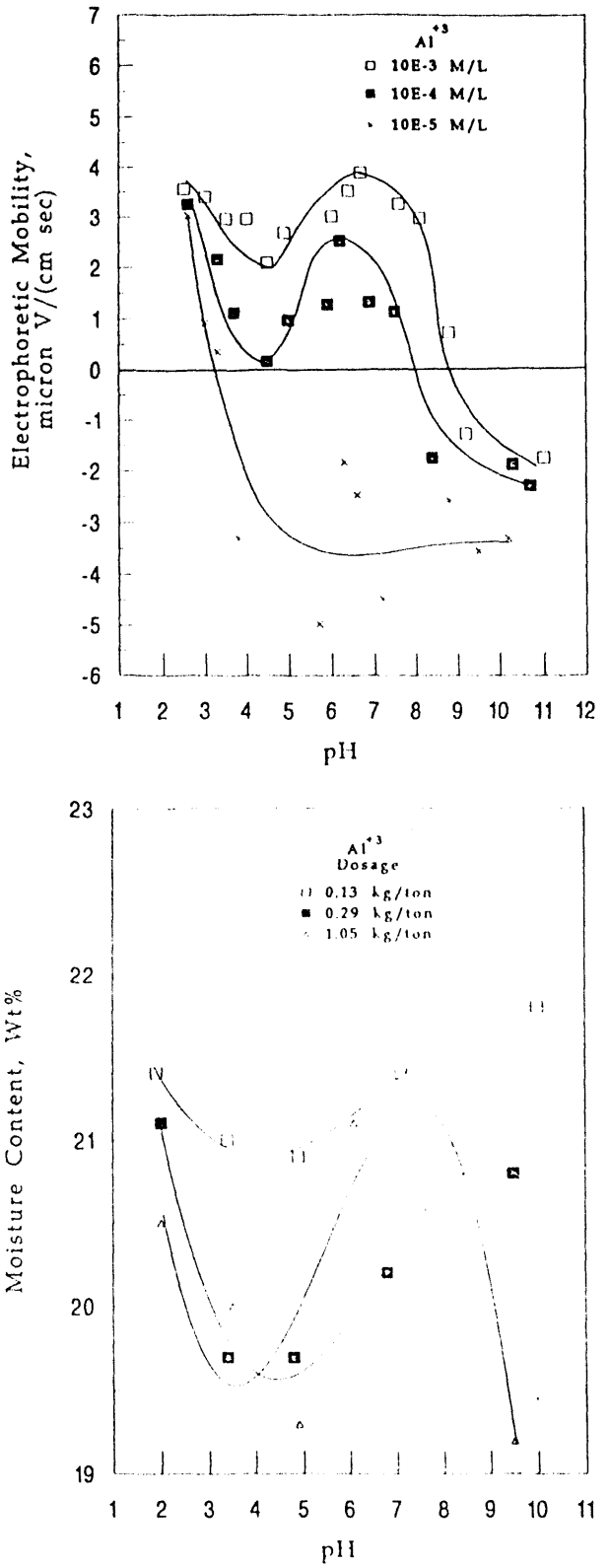

Figure 10. Effect of pH with presence of aluminum ions

(a) Electrophoretic mobility

(b) Cake moisture

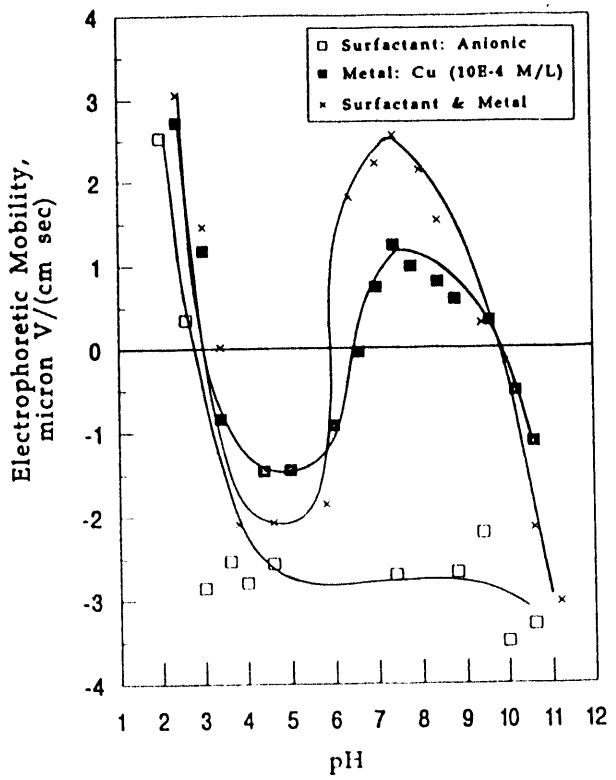

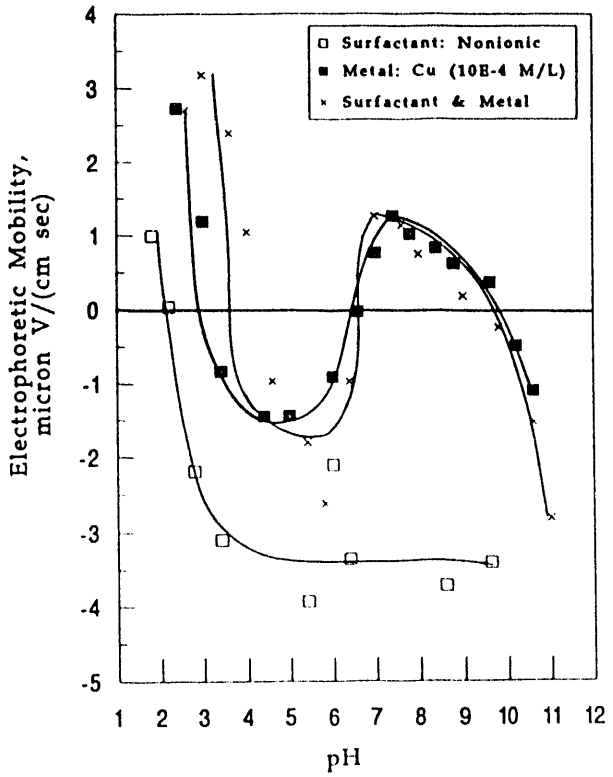

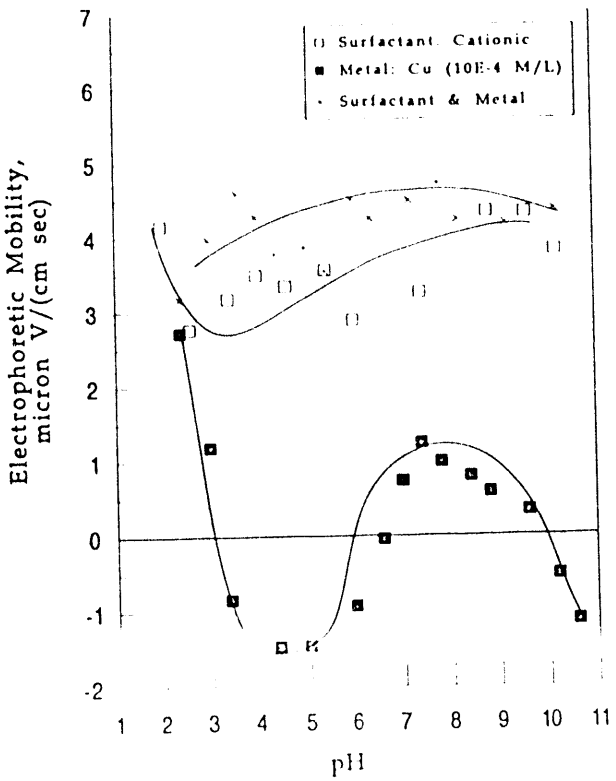

Figure 11. Electrophoretic mobility of coal with presence of copper ions, surfactants and their combinations

(a) Anionic surfactant

(b) Nonionic surfactant

(c) Cationic surfactant

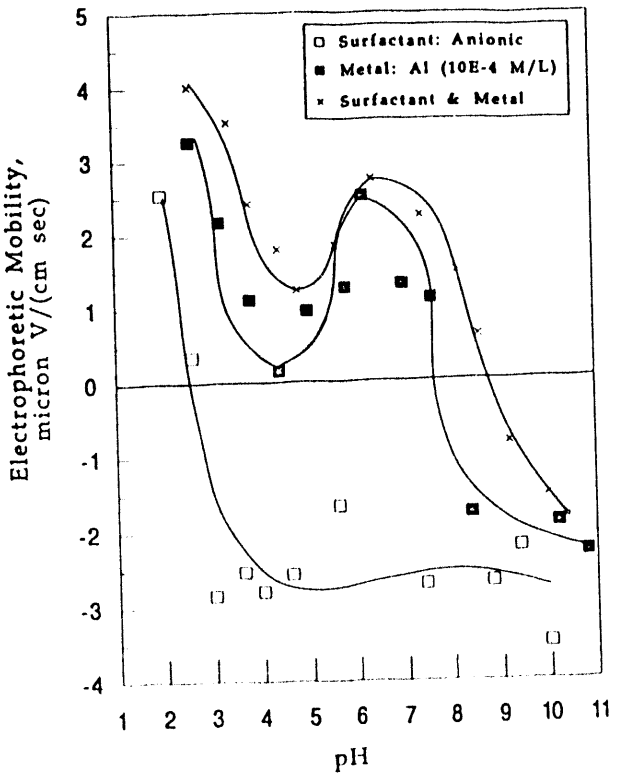

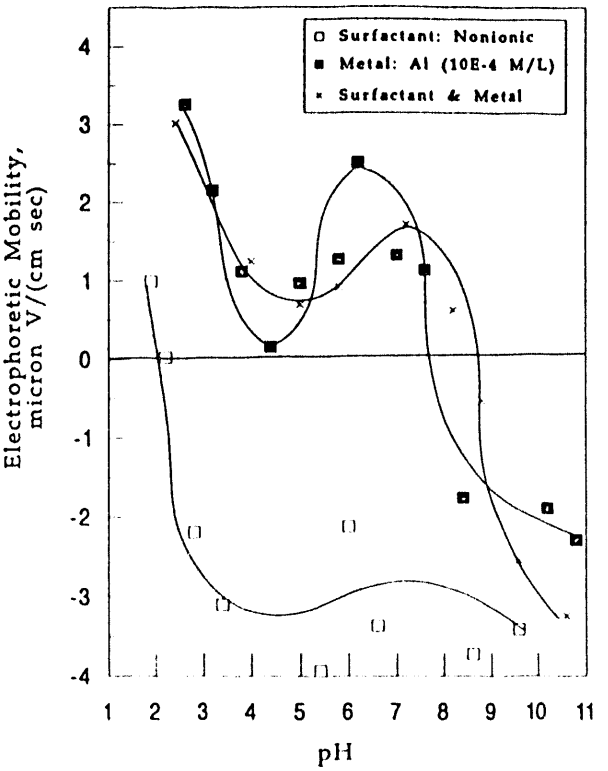

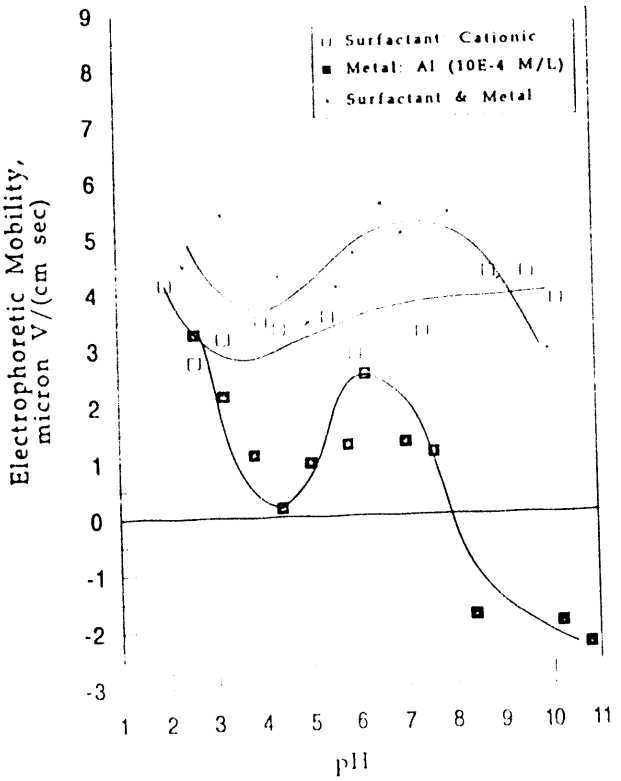

Figure 12. Electrophoretic mobility of coal with presence of aluminum ions, surfactants and their combinations

(a) Anionic surfactant

(b) Nonionic surfactant

(c) Cationic surfactant

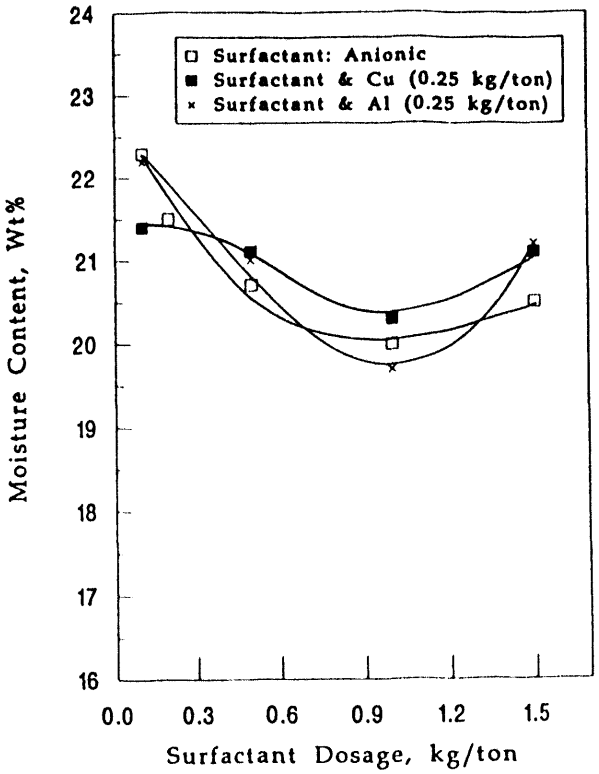

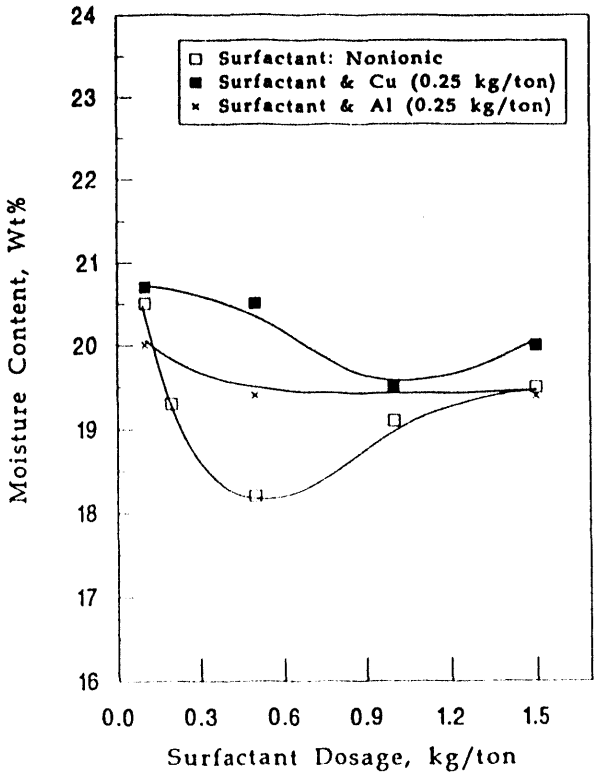

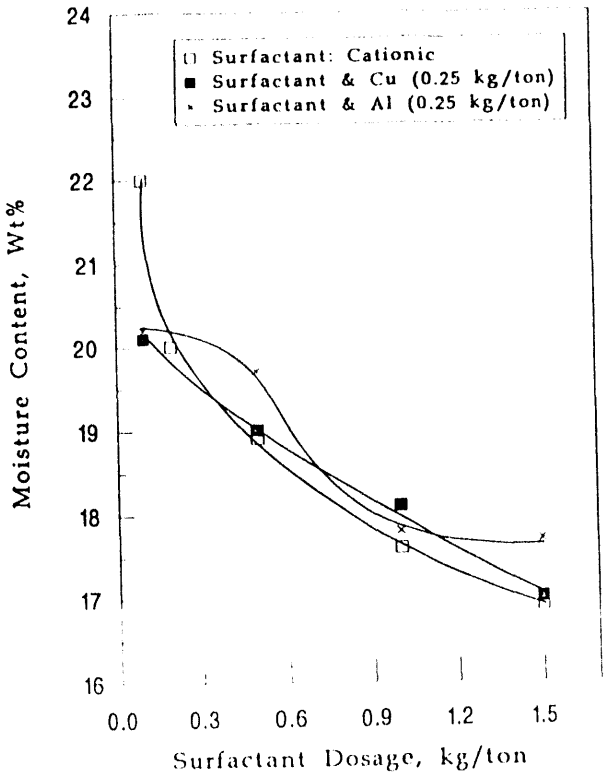

Figure 13. Combined effect of metal ions and surfactants on cake moisture

(a) Anionic surfactant

(b) Nonionic surfactant

(c) Cationic surfactant

DATE
FILMED
2/28/94
END